International Journal of Thermal Sciences 48 (2009) 1423–1431

Contents lists available at ScienceDirect

International Journal of Thermal Sciences

www.elsevier.com/locate/ijts

Effects of CO_2 dilution on the interactions of a CH_4–air nonpremixed jet flame with a single vortex

Cheol-Hong Hwang [a,1], Chang Bo Oh [b], Chang-Eon Lee [a,*]

[a] School of Mechanical Engineering, Inha University, 253, Yonghyun-dong, Nam-gu, Incheon 402-751, Republic of Korea
[b] Division of Safety Engineering, Pukyong National University, Busan 608-739, Republic of Korea

ARTICLE INFO

Article history:
Received 25 April 2008
Received in revised form 4 October 2008
Accepted 6 November 2008
Available online 28 November 2008

Keywords:
CO_2 dilution
Flame-vortex interaction
Nonpremixed flame
Vorticity transport mechanism

ABSTRACT

We carried out numerical simulations to understand how CO_2 dilution in either fuel or oxidizer stream changes the flame-vortex interactions in terms of hydrodynamic effects in CH_4–air nonpremixed jet flames. The simulation used a time-dependent, axisymmetric computational model and a low Mach number approximation. Reaction rates were calculated from a two-step global reaction mechanism that considered six species. Studies were conducted with fixed initial velocities for three different cases of CO_2 introduction: (1) without dilution, (2) dilution in a fuel stream, and (3) dilution in an oxidizer stream. A single vortex was generated by an axisymmetric jet driven of cold fuel, after a flame development was reached to quasi steady-state condition. The simulation shows that CO_2 dilution in a fuel stream leads to a slightly increased vortex radius and more entrainment of surrounding fluids compared to the other dilution methods tested. Thus, dilution of CO_2 in a fuel stream enhances the mixing inside a single vortex and increases the stretching of the flame surface. The vorticity transport equation budgets were examined to reveal the mechanisms of vortex formation in the presence of CO_2. In the stage of vortex formation, vortex production due to baroclinic torque and vortex destruction due to volumetric expansion were found to be greater in the case of CO_2 dilution in a fuel stream than in the other dilution cases. However, after vortex formation, there terms showed the opposite tendencies.

1. Introduction

Carbon dioxide (CO_2), produced by the burning of hydrocarbon fuels, is widely known as a greenhouse gas. Recently, attention has focused on reducing CO_2 emission by increasing the thermal efficiency of combustion systems. Oxygen-enriched combustion [1] as a CO_2 reduction technique is believed to hold tremendous promise for protecting the environment as well as saving energy. However, since flame temperature increases with the oxygen concentration ratio in oxidizer, controlling the flame temperature in oxygen-enriched combustion is necessary for maintaining the thermal stability of the combustor. Often, an exhaust gas including CO_2 is introduced into either the fuel stream or the oxidizer stream. Other examples in which CO_2 is used in combustion are the exhaust gas recirculation (EGR) technique for NO_x reduction in industrial burner applications and the utilization of landfill gas (LFG) [2], which contains considerable quantities of CO_2. CO_2 dilution in the fuel or oxidizer streams is thought to affect strongly the characteristics of flow and reaction in a reacting flow field. It also leads to significant changes in flame structure and flame stability as well as pollutant emissions of NO_x, CO, and soot.

Various published reports have examined the effects of CO_2 dilution in fuel or oxidizer streams. Bae et al. [3] and Satio et al. [4] recently reported the effects of CO_2 dilution on flame stability and extinction behavior for a laminar jet flame. Lee et al. [5] studied the effects of including CO_2 in an oxidizer stream on flame structure and NO_x formation in a CH_4–air counterflow nonpremixed flame. Feese et al. [6] discussed the NO_x emission and detailed flame chemistry depending on whether the dilution was done in the fuel stream or the oxidizer stream. Liu et al. [7] studied the chemical effects of CO_2 as an additive on soot and NO_x formations in an ethylene nonpremixed flame. All of these studies focused on the molecular transport and chemical kinetic characteristics of CO_2 dilution, which they sought to explain mainly through chemical and thermal effects.

In addition to these effects, however, the hydrodynamic effects due to CO_2 dilution can change many fundamental phenomena such as entrainment and mixing, local extinction due to flame stretching, diffusion and differential diffusion and vorticity distribution in a reacting flow field [8]. In particular, whether CO_2 dilution is carried out in the fuel stream or the oxidizer stream is expected to strongly influence these many phenomena. However,

* Corresponding author. Tel.: +82 32 860 7323; fax: +82 32 868 1716.
E-mail address: chelee@inha.ac.kr (C.-E. Lee).
[1] Current address: National Institute of Standards and Technology, Gaithersburg, MD 20899-8663, USA.

1290-0729/$ – see front matter
doi:10.1016/j.ijthermalsci.2008.11.003

few studies on CO_2 dilution have addressed such as hydrodynamic effect.

To identify the effect of CO_2 dilution on the dynamic behavior of turbulent flame, an understanding of flame-vortex interactions is required since a turbulent flame can be viewed as an ensemble of flame-vortex interactions. The flame-vortex interactions contains many of the fundamental aspects of the coupling between fluid dynamics and combustion that could be investigated with more controllable conditions than are possible under direct investigations of turbulent flames [9]. In addition, the interactions between the large vortices generated in the shear layer and flame zone are of essential importance because they are related to various aspects of combustion phenomena such as instability and transient effects of a turbulent flame, flame stability, and local extinction [10]. Thus, many investigations have looked closely at the interactions between flames and single vortices; this system has characteristics similar to those of turbulent flames [11,12].

In the present study, numerical calculations were preformed for a single vortex generated in a CH_4–air nonpremixed jet flame. To identify the effect of CO_2 dilution on flame-vortex interactions, CO_2 was diluted in either the fuel or oxidizer stream. The analyses of vortex dynamics interacting with a flame were carried out to understand how CO_2 dilution in either fuel or oxidizer stream changes the vorticity field globally.

2. Description of numerical model

2.1. Governing equations and numerical methods

This study used a time-dependent axisymmetric configuration to accommodate an unsteady nonpremixed jet flame. A set of model-free equations with a low Mach number approximation [13] was used. The resulting conservation equations are written in Eqs. (1)–(5).

$$\frac{\partial \rho}{\partial t} + \nabla \cdot (\rho \boldsymbol{u}) = 0 \tag{1}$$

$$\frac{\partial (\rho \boldsymbol{u})}{\partial t} + \nabla \cdot (\rho \boldsymbol{u}\boldsymbol{u}) = -\nabla p_1 + \nabla \cdot \mu\left[(\nabla \boldsymbol{u}) + (\nabla \boldsymbol{u})^T - \frac{2}{3}(\nabla \cdot \boldsymbol{u})\boldsymbol{I}\right] + (\rho - \rho_0)\boldsymbol{g}$$

$$\frac{(\partial \rho Y_i)}{\partial t} + \nabla \cdot (\rho \boldsymbol{u} Y_i) = \nabla \cdot (\rho D_{im} \nabla Y_i) + W_i \dot{\omega}_i \tag{2}$$

$$(i = 1, 2, \ldots, N) \tag{3}$$

$$\rho c_p \left(\frac{\partial T}{\partial t} + \boldsymbol{u} \cdot \nabla T \right) = \nabla \cdot (\lambda \nabla T) + \rho \sum_{i=1}^{N} (c_{pi} D_{im} \nabla Y_i \cdot \nabla T) - \sum_{i=1}^{N} W_i h_i^0 \dot{\omega}_i \tag{4}$$

$$p_0 = \rho R_0 T \sum_{i=1}^{N} \left(\frac{Y_i}{W_i} \right) \tag{5}$$

where, p_0 and p_1 are the thermodynamic and hydrodynamic pressures, respectively, and have the relationship of $p = p_0 + p_1$; $\boldsymbol{u}$ is the velocity vector; T is the temperature; ρ is the density of mixture; ρ_0 is the density of ambient air at standard state condition; R_0 is the universal gas constant; and Y_i, h_i^0, $\dot{\omega}_i$, and c_{pi}, are the mass fraction, heat of formation, production rate, and specific heat of species i, respectively. In addition, D_{im} denote the mixture-averaged diffusion coefficients of species i, which are calculated from the following averaging formulation:

$$D_{im} = \frac{1 - Y_i}{\sum_{j \neq i}^{N} X_j / D_{ji}} \tag{6}$$

where X_j is mole fraction and D_{ji} are the binary diffusion coefficients obtained from the collision integrals. The Soret and Dufour effects were not considered in this study. The detailed descriptions on the transport model can be found in [14].

QUICK [15] and second-order central difference schemes were used to discretize the convection and diffusion terms of the governing equations. A predictor-corrector scheme nearly identical to that of Najm et al. [16] was used for time integration of the governing equations. Efficient algebraic relaxation for the velocity-pressure correction was performed using the HSMAC method [17]. The CHEMKIN-II [18] and TRANFIT [14] packages were adopted for the calculation of thermodynamic and transport properties. The detailed numerical scheme can be found elsewhere [19,20].

The nonpremixed flame considered in this study was developed from a 10 mm-diameter fuel nozzle with a rim thickness of 0.46 mm. Fuel and oxidizer were supplied at atmospheric pressure with an inlet temperature of 298 K. The mean velocities of fuel and oxidizer at nozzle exit were set to be 0.6 and 0.2 m/s, respectively. A top-hat velocity profile similar to that of a contoured nozzle was applied to the nozzle exit. The top-hat velocity profile at the nozzle exit was given by:

$$u(r) = u_0 \left[\frac{1}{2} - \frac{1}{2} \tanh\left\{ 10\left(\frac{r}{R} - 1 \right) \right\} \right] \tag{7}$$

where r is the radial distance; R, the radius of fuel nozzle; and u_0, the representative exit velocity of the fuel. The velocity profile of oxidizer was also assigned a uniform distribution except near a nozzle.

A numerical calculation was carried out on a domain size of $L_x \times L_r = 85$ mm $\times$ 70 mm ($x = -5$–80 mm and $r = 0$–70 mm). A non-uniform grid system having $N_x \times N_r = 240 \times 160$ grid points was used for axial and radial direction to achieve higher resolution in the regions of steep gradients. The schematic of the calculation domain and details of each boundary condition (BC) are shown in Fig. 1. The BCs at the central and lateral boundaries were taken to be axisymmetric and slip, respectively. At the wall of a noz-

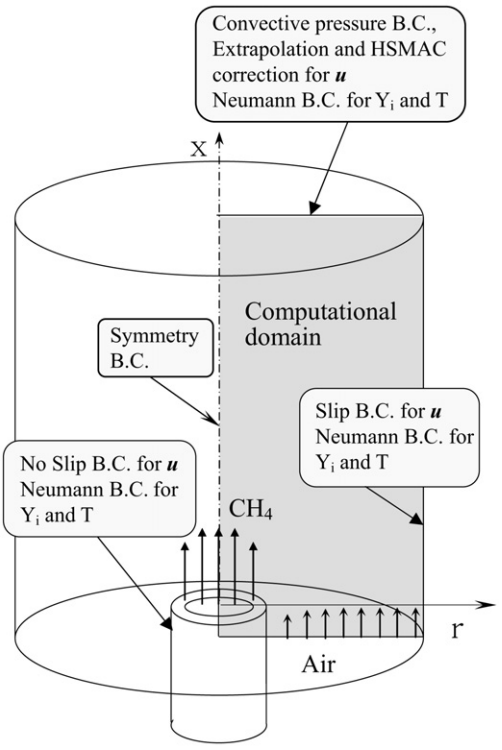

Fig. 1. Computational domain and boundary conditions.

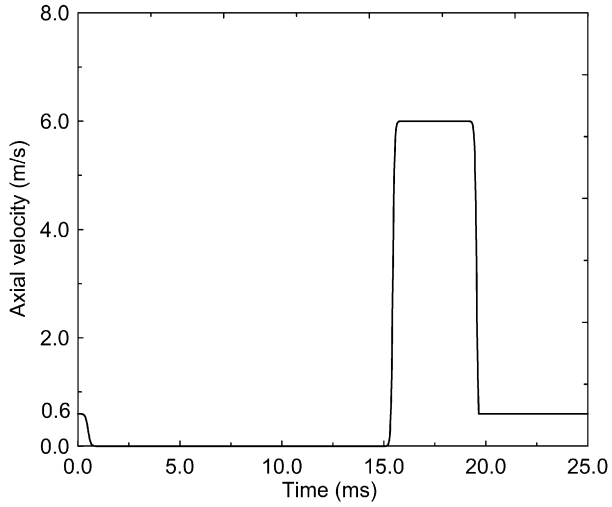

Fig. 2. Velocity program at the exit of fuel nozzle for the generation of single vortex.

zle, a no-slip BC was also used. The Neumann BC was imposed for the species and temperature at these boundaries. A new BC was devised to serve as the outflow BC of an unsteady jet flame. Thus, the outflow boundary was characterized with the convective BC for pressure defined by Eq. (8). Furthermore, the velocities at the outflow boundary were evaluated through extrapolation. The velocity-pressure correction was then conducted using an HSMAC method at all grid points. This allowed simultaneous mass conservation for each grid point and for the entire solution domain.

$$\frac{\partial p_1}{\partial t} + u_0 \frac{\partial p_1}{\partial x} = 0 \tag{8}$$

In this study, a single vortex was generated by an axisymmetric jet, which was made by an impulse of cold fuel after a flame development was reached to quasi steady-state condition. In an unsteady jet flame, the outer vortex, formed by buoyancy-driven instability, moves downstream periodically through the processes of bulge and roll-up. To ensure identical control of the interactions between flame and outer vortex on single vortex dynamics, a single vortex was generated at the instant that the outer vortex moved completely through the computational domain. The velocity program used to generate the single vortex at the exit of the fuel nozzle is shown in Fig. 2.

The two-step global reaction mechanism for methane oxidation originally proposed by Dupont et al. [21] was used in this study. This mechanism consists of six species (CH_4, CO, CO_2, H_2O, O_2, and N_2), and the N_2 species is present as an inert gas. The reaction mechanism and reaction rates are given by:

$$CH_4 + \frac{3}{2}O_2 \rightarrow CO + 2H_2O \tag{R1}$$

$$CO + \frac{1}{2}O_2 \rightarrow CO_2 \tag{R2}$$

$$\omega_1 = 10^{10.0} \exp\left(\frac{-12{,}019}{T}\right)[CH_4]^{1.0}[O_2]^{1.0} \tag{9}$$

$$\omega_2 = 10^{10.0} \exp\left(\frac{-12{,}019}{T}\right)[CO]^{1.0}[O_2]^{1.0} \tag{10}$$

[ ] denotes the species concentration (kmol/m^3). The reaction was initiated by applying a high ignition temperature of 1300 K to the small area near the nozzle exit when the fuel jet had proceeded to approximately one-third of the solution domain. The advance time step (Δt) was fixed at 5 μs to ensure stable convergence.

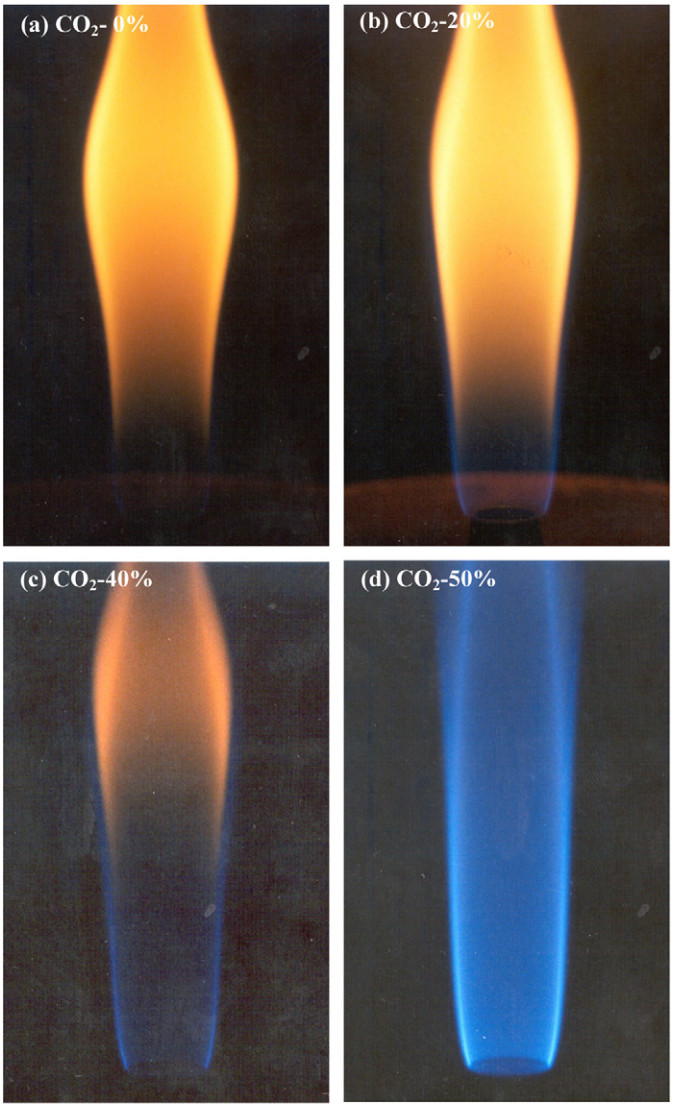

Fig. 3. Instantaneous flame shape with CO_2 addition in fuel stream by direct photography. (For interpretation of the references to color in this figure legend, the reader is referred to the web version of this article.)

2.2. Flame shape with CO_2 dilution

To determine the amount of CO_2 to be mixed in the fuel and oxidizer streams, direct photography was used to visualize the instantaneous flame shapes with the CO_2 addition in the fuel stream as shown in Fig. 3. This experiment was conducted under conditions equivalent to those used in the numerical simulation. The flame gradually gains a blue color with increasing addition of CO_2. When the composition (by volume) of CO_2 in the fluid supplied in the fuel nozzle reaches 50%, the flame lifts up from the nozzle and becomes unstable. In the case of 40% CO_2, however, the flame is stable and it displays an almost blue color, except for the flame bulge that expands in the radial direction (Fig. 3(c)). Thus, CO_2 at a concentration of 40% by volume in the fuel stream was applied in our simulations to study the effect of CO_2 dilution on the interactions of a CH_4–air nonpremixed jet flame with a single vortex.

Table 1 provides relevant information for each of the case studies. No dilution, which used pure CH_4 and air as fuel and oxidizer, respectively, was considered a reference case. Fuel dilution, corresponding to the addition of CO_2 to the fuel stream, was examined to study the effect of CO_2 dilution on a single vortex generated

Table 1
Compositions of fuel and oxidizer stream for CO_2 dilution at inlet boundary.

	Fuel stream (Mole fraction)		Oxidizer stream (Mole fraction)			Equilibrium temp. (K)
	CH_4	CO_2	O_2	N_2	CO_2	
No dilution	1.0	0	0.210	0.790	0	2246.6
Fuel dilution	0.6	0.4	0.210	0.790	0	2103.9
Air dilution	1.0	0	0.196	0.738	0.066	2103.9

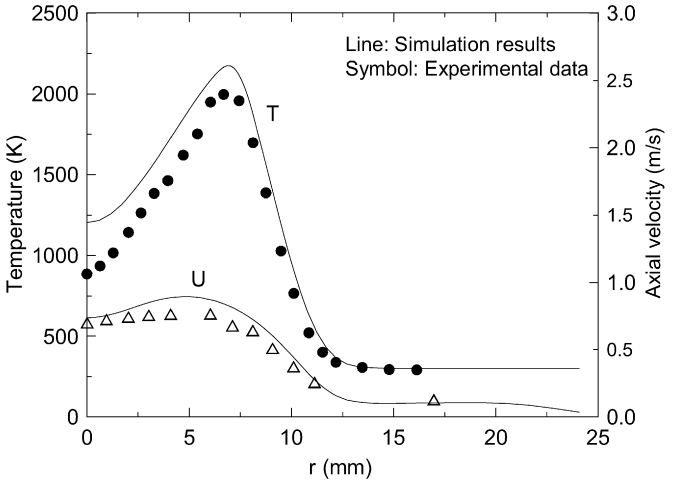

(a) Temperature and axial velocity at $x = 12$ mm

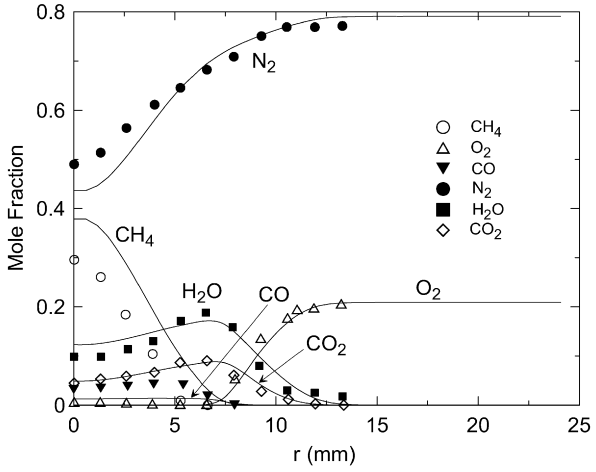

(b) Major species concentration at $x = 12$ mm

Fig. 4. Comparison of simulation results and experiment data for the CH_4–air laminar nonpremixed jet flame.

from a fuel nozzle. In the case of air dilution, the amount of CO_2 dilution was decided to obtain the same adiabatic equilibrium temperature as in the case of fuel dilution to identify the influence of heat on vortex dynamics.

2.3. Validations numerical code

The present numerical code was validated for temperature, major species concentrations and axial velocity profile for a CH_4–air laminar nonpremixed jet flame by comparing with the experiment data by Peters et al. [22]. The diameters of fuel and ambient air nozzle are 12.7 and 50.8 mm, respectively. The average velocities at the fuel and ambient air nozzle exits are 4.5 and 9.88 cm/s, respectively. The comparison between the simulation results and experiment data at an axial location of $x = 12$ mm is shown in Fig. 4. The overall trend of temperature and axial velocity were well predicted by the simulation except for the slightly over-predicted temperature at the region of $r \leqslant 8$ mm. It is also seen from the figure that the predicted species concentrations are in good agreement with the measurements. Considering that the radiative heat loss was neglected and a relatively simple two-step global reaction mechanism was used in the simulation, the simulation results were found to be within reason. In addition, the prediction performance of the numerical code used in this study was also validated for counterflow flames [19,23,24] and jet flames interacting with vortices [20] by comparing the main features with experiments. Thus, it can be concluded that the present numerical code is suitable for investigating the interactions of CH_4–air nonpremixed jet flame with a single vortex.

3. Results and discussions

3.1. Dynamic behavior of a single vortex

To study the dynamic behaviors and mixing characteristics of a single vortex, the evolutions of temperature and flame surface of unsteady nonpremixed jet flames were followed over time for each dilution scenario as shown in Fig. 5. Five representative snapshots produced by the velocity program in Fig. 3 are shown. Each contour is plotted for temperatures above 500 K. The dashed lines in the figure correspond to the flame surface and indicate the location of the stoichiometric mixture fraction. The mixture fraction is defined as follows:

$$Z = \frac{\nu Y_F - Y_{O_2} + Y_{O_2,2}}{\nu Y_{F,1} + Y_{O_2,2}} \tag{11}$$

where $\nu = \nu'_{O_2} W_{O_2} / \nu'_F W_F$ is the stoichiometric oxidizer-to-fuel mass ratio; the subscript O_2 and F indicate oxidizer and fuel, respectively; ν' is the stoichiometric coefficients; and the subscripts 1 and 2 correspond to the initial fuel stream and air stream, respectively.

Fig. 5(a) shows the results for no dilution, which used pure CH_4 and air as fuel and oxidizer, respectively. The outer vortex, generated by buoyancy-driven instability, starts to bulge outward in the region of $x = 50$ mm and to move downstream. At 18.75 ms, the instant when high-speed fluid is injected, the surrounding fluids located near the flame surface are entrained to the inside of the single vortex while the inner single vortex is generated. At 23.75 ms, fuel is supplied by 0.6 m/s again as shown in Fig. 2 and, the single vortex radius and the entrainment of surrounding fluid to the inside of the vortex increase further. Although the flame surface is significantly stretched, no local extinction is observed. Subsequent images in the series show that mixing inside the vortex is enhanced and that the temperature distribution inside the vortex appears to approach uniformity. Furthermore, disturbance of the flow field moves the flame surface located behind the vortex into the central axis, which instantaneously causes cutoff of the high-speed fluids.

The results for CO_2 dilution in the fuel stream are shown in Fig. 5(b). The case of fuel dilution shifts the location of the flame surface to the inside compared to the case of no dilution at 0.0 ms. Comparison of the dynamic behavior of a single vortex in the no dilution and fuel dilution shows that, at 18.75 and 23.75 ms, the fuel dilution involves a larger vortex radius and the entrainment of more mass flux to the inside of the vortex at a temperature greater than 500 K. This is caused by the fact that CO_2 dilution of the fuel stream changes the density, which significantly increases the momentum flux. At 28.75 ms, the temperature inside the vortex exceeds 500 K faster than in the no dilution. The flame surface in fuel dilution is also significantly more distorted than in no dilution due to the higher momentum flux. Thus, the interaction between

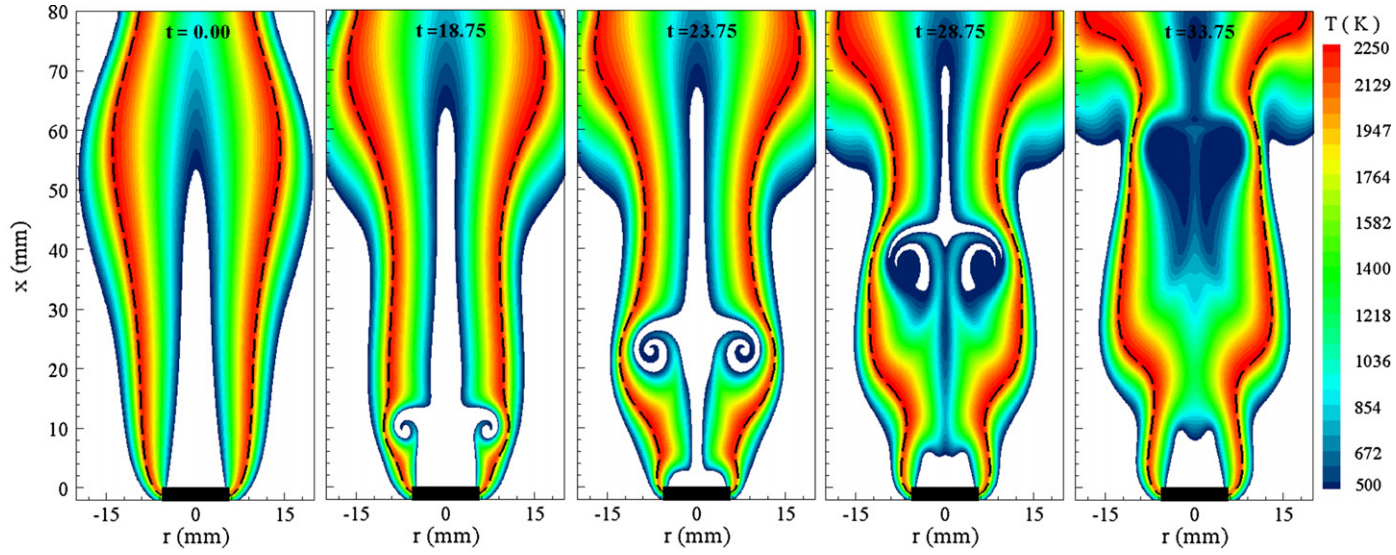

(a) No dilution

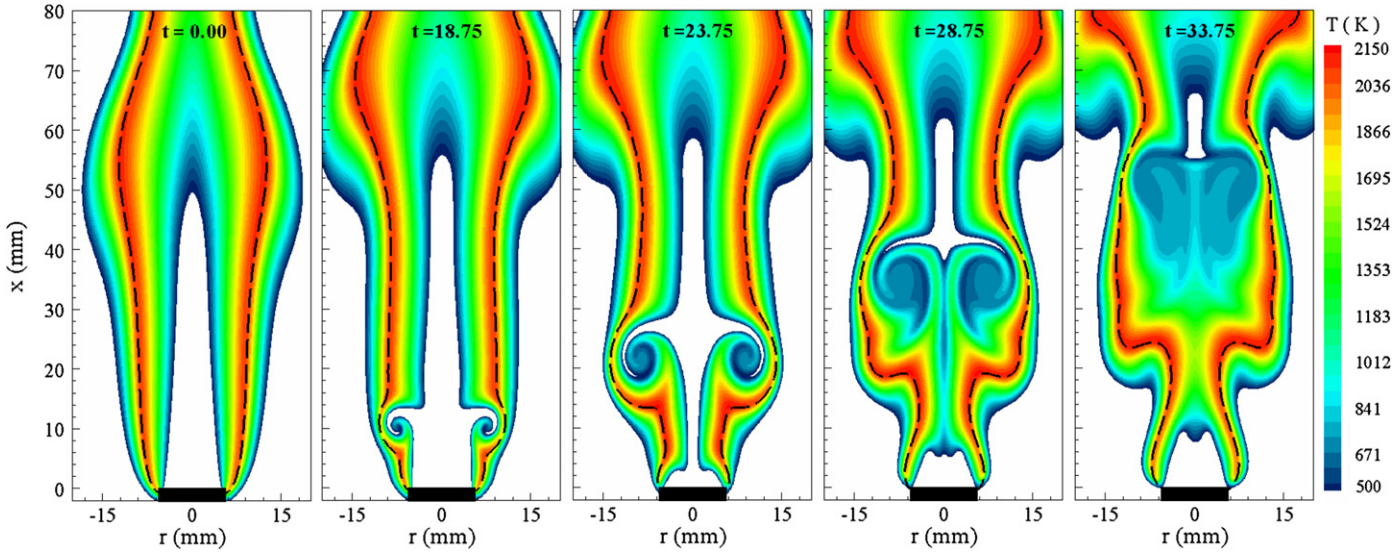

(b) Fuel + CO_2

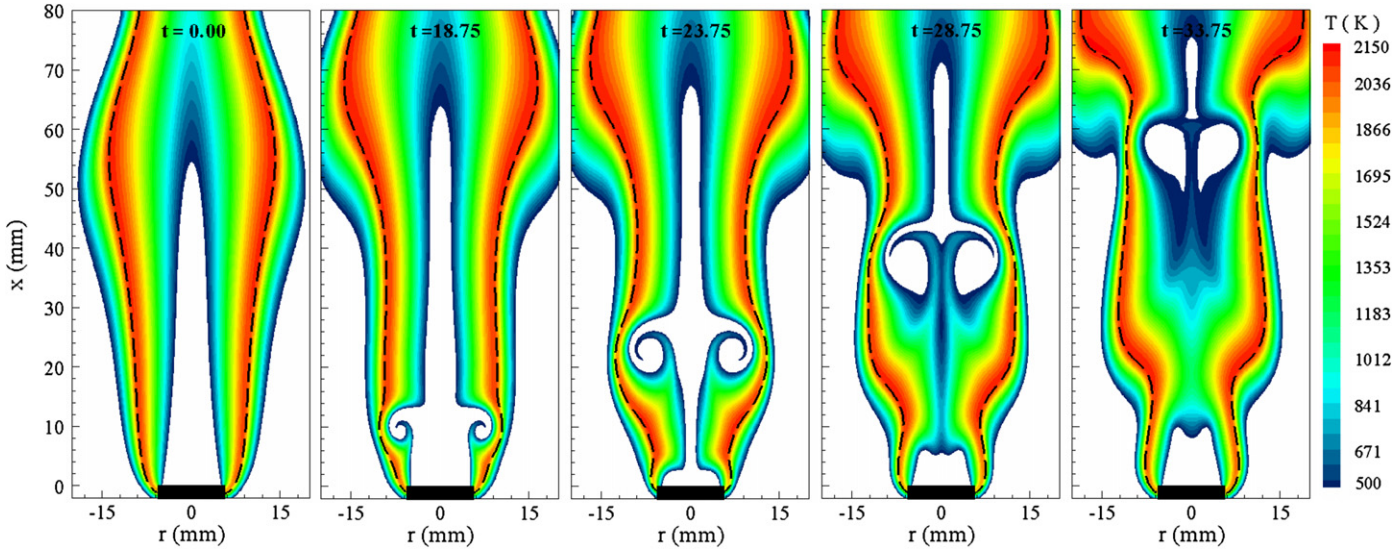

(c) Air + CO_2

Fig. 5. Temporal evolutions of temperature and flame surface for no dilution, fuel dilution and air dilution of CO_2.

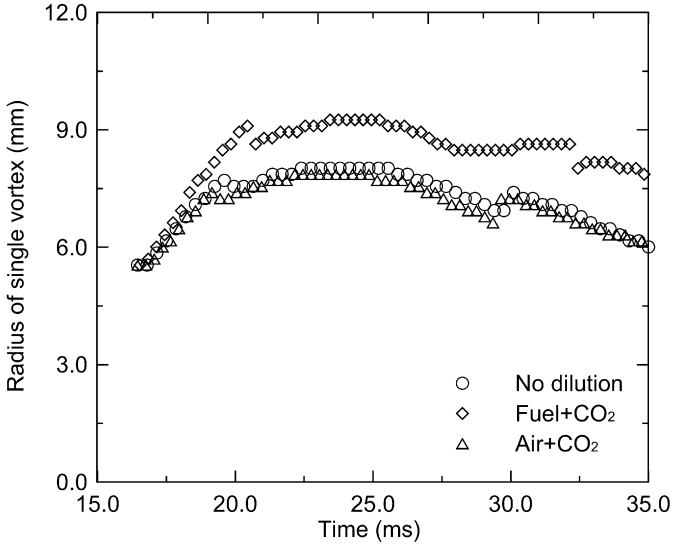

Fig. 6. Radius of single vortex over time for dilution conditions.

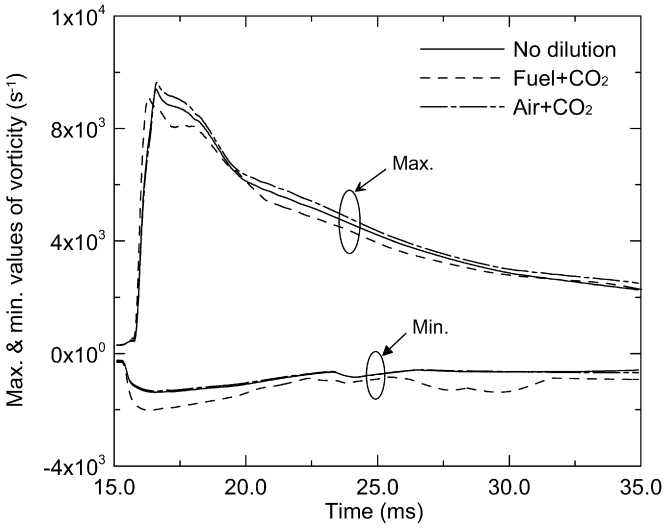

Fig. 7. Maximum and minimum values of vorticity over time for dilution conditions.

flame and vortex appears to be significant when CO_2 dilution occurs via the fuel stream.

Fig. 5(c) shows the results for CO_2 dilution in the oxidizer stream. At 0.0 ms, the locations of the flame surface are almost identical to those in the no dilution. This is because the differences in stoichiometric mixture fraction are very small between the no dilution and air dilution. That is, although the adiabatic flame temperature in air dilution is lower than in no dilution by approximately 140 K, the amount of CO_2 diluted in the oxidizer stream (mole fraction, 0.066) for air dilution is very small, as presented in Table 1. At 23.75 and 28.75 ms, the flame shapes and single vortex outlines are similar to those in no dilution, but the mixing effect inside the vortex is very weak compared to the other cases. This result can be attributed to the higher weight of the oxidizer stream due to CO_2 dilution, even though the fuel stream in air dilution has the same momentum flux as in no dilution.

Fig. 6 shows the single vortex radius for three dilution conditions as a function of time. The single vortex radius is calculated from the location of the core with the maximum vorticity. The single vortex radii in the no dilution and air dilution behave nearly identically over time. In these two dilution conditions, the single vortex radii increase with time then gradually decrease at 25.0 ms. In the fuel dilution, in which CO_2 is included in the fuel stream, the single vortex radius is larger than in the other dilution conditions. This can be attributed to greater entrainment of high-temperature fluid due to the high momentum flux of the fuel stream, as described in Fig. 5. Furthermore, the vortex in fuel dilution appears to affect flame behavior significantly, since the increase in vortex radius stretches the flame surface.

The maximum and minimum values of vorticity over the calculation domain over time are shown in Fig. 7. The vorticity increases up to a maximum value during vortex formation, then gradually decreases with time. The time histories of vorticity are nearly identical for the no dilution and air dilution. In contrast, the maximum and minimum vorticity values in the fuel dilution are lower than in the other dilution conditions, and they fluctuate irregularly over time. These results imply that CO_2 dilution in the fuel stream makes the behavior of the combustion field more complicated.

From Figs. 6 and 7, it can be known that the vortex radius in fuel dilution is larger than in other dilution conditions, whereas the maximum and minimum values of vorticity are lower than in other conditions. These opposite tendencies of vortex radius and vorticity magnitude cannot provide the consistent analysis to understand how much CO_2 dilution affects flame-vortex interactions in terms of hydrodynamic effects. Thus, we adopt the additional parameters of total circulation and hydrodynamic impulse over the entire computational domain, as shown in Figs. 8 and 9.

To determine how CO_2 dilution alters the vorticity field globally, the total circulation of the flow field with time is shown in Fig. 8. Total circulation is the measure of the strength of the vorticity field, and it can be calculated using Eq. (12):

$$\Gamma = \int_A \omega_\theta \, dA \tag{12}$$

where ω_θ denotes the azimuthal component of the vorticity. The integration for this equation is performed over the entire computational domain area, as shown in Fig. 1.

The total circulation is normalized by the total circulation at 0.0 ms (Γ_0) to provide a meaningful comparison between the results for each dilution condition since a flow field already has some finite total circulation before the formation of a single vortex. For all dilution conditions, the circulation increases during the formation of a single vortex, sharply decreases when a forced fuel jet is cut off corresponding to near 20.0 ms, and then gradually increases. The circulation value at 20.0 ms for the fuel dilution is significantly larger than in the other dilution conditions. This result can be explained from the vortex radius and the values of maximum and minimum vorticity. In other words, this means that the area including a high-order vorticity magnitude increase more than in the other dilution conditions, although the maximum and minimum vorticity values are smaller than those of the other conditions. Meanwhile, total circulation is nearly identical for the no dilution and air dilution, except for a small discrepancy after 25.0 ms.

In Fig. 5, we indicated visually that the entrainment and mixing of surrounding fluids inside the vortex change significantly due to the momentum difference with CO_2 dilution in the fuel or the oxidizer streams. Hydrodynamic impulse which plays the part of vortex momentum, is thought to be an adequate parameter for quantifying the effect of momentum difference on vortex dynamics. The hydrodynamic impulse is expressed in three-dimensional motion as shown in Eq. (13). It can be written, however, for two spatial dimensions as Eq. (14) since the hydrodynamic impulse only validates the component of axial direction in two-dimensional cylindrical coordinates:

$$\vec{I} = \frac{1}{2}\int_V \rho \vec{r} \times \vec{\omega} \, dV \tag{13}$$

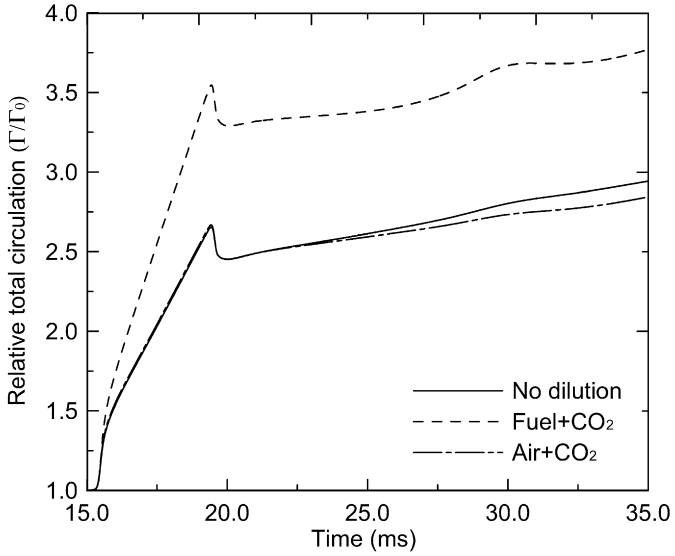

Fig. 8. Relative total circulation over time for dilution conditions.

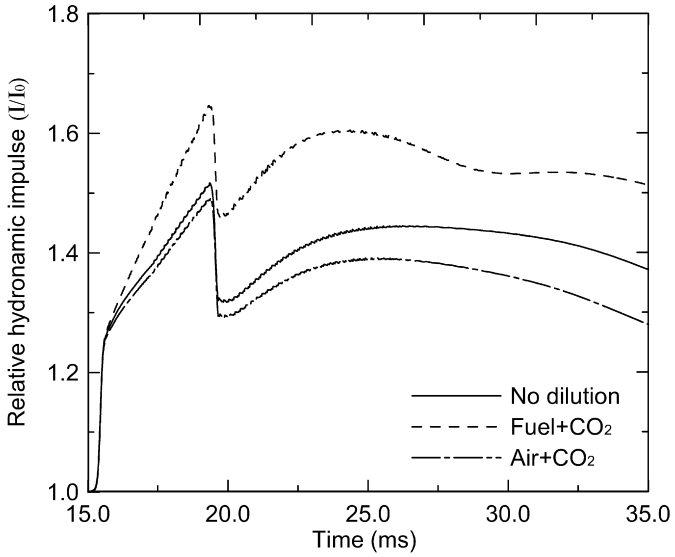

Fig. 9. Relative hydrodynamic impulse over time for dilution conditions.

$$I_x = \pi \int_A \rho \omega_\theta r^2 \, dA \tag{14}$$

where $\vec{r}$ is the position vector of a point in the flow field. Henceforth, when the term impulse is used, it refers to the axial component of $\vec{I}$, and it will be referred to as I.

Fig. 9 shows the evolution of hydrodynamic impulse over time in three dilution conditions as an indication of the entrainment and mixing behavior inside the vortex. The hydrodynamic impulse in the fuel dilution, in which CO_2 is added in the fuel stream, varies rapidly over time, while that of the air dilution varies most slowly among the three dilution conditions. Thus, in the case of CO_2 dilution in the fuel stream, the increase in entrainment of surrounding fluids near the flame surface appears to promote mixing inside the vortex.

3.2. Vorticity transport mechanisms

To determine how CO_2 dilution in the fuel and oxidizer streams changes the vorticity field globally, contributions to the total circulation were calculated by integrating each term in the vorticity transport equation over the computational domain, as shown in Fig. 10. For a two-dimensional flow field, the vorticity transport equation may be written as:

$$\frac{\partial \omega_\theta}{\partial t} = -(\boldsymbol{u}\cdot\nabla)\omega_\theta + (\omega_\theta\cdot\nabla)\boldsymbol{u} - \omega_\theta(\nabla\cdot\boldsymbol{u}) + \frac{1}{\rho^2}(\nabla\rho\times\nabla p) + \nabla\times\left(\frac{\rho-\rho_\infty}{\rho}\right)\boldsymbol{g} + (\text{Viscosity-related terms}) \tag{15}$$

In this equation, the first term on the right side is the convective term, and the second term is referred to as the stretching term having an inherently three-dimensional phenomenon. However, since this calculation is limited to a two-dimensional flow field, only the stretching effect in the θ-direction is considered in the present study. The third term, called the volumetric expansion term, corresponds to the reduction in vorticity arising from fluid expansion. The fourth term is the baroclinic torque caused by the non-collinearity of the density and pressure gradients, which plays an important role in vortex generation when the density changes significantly, such as in the reacting flow. The gravitational term resulting from the interactions of the radial density gradient $(\partial\rho/\partial r)$ and gravitational acceleration is represented by the penultimate term. Because of the sign change of $\partial\rho/\partial r$ across the reaction zone, it takes a negative sign on the inner side and a positive sign on the outer side of a flame surface. This term contributes mainly to an increase in flow vortical level. The last terms on the right-hand side are referred to as the viscosity-related terms, which consist of the vorticity diffusion term due to the action of viscosity and the terms due to shear stress variations in a density gradient field. These terms are calculated from the difference between the left- and right-hand sides of Eq. (15). In addition, the $\partial\omega_\theta/\partial t$ term in Eq. (15) is related to the change in total circulation as follows:

$$\frac{\partial \Gamma}{\partial t} = \int_A \frac{\partial \omega_\theta}{\partial t}\, dA \tag{16}$$

The $\partial\omega_\theta/\partial t$ term in Eq. (16) can be replaced by the right-hand side of Eq. (15). Therefore, the integration of each term on the right-hand side of the vorticity transport equation over the computational domain gives the contribution of each term to the change in total circulation.

Fig. 10(a) shows the contributions of vortex stretching to the total circulation over time for all dilution conditions. The stretching term can be expressed as $\omega_\theta(v/r)$ since the stretching effect in the θ-direction is valid only in a two-dimensional cylindrical coordinate system, as previously mentioned. This term depends on both the radial velocity and the vorticity ω_θ, which is typically positive. The stretching effects for all dilution conditions rapidly increase near 15.0 ms, since the radial velocity v is typically positive when a vortex is formed from the fuel nozzle. Meanwhile, the contribution of vortex stretching decreases sharply at the high-velocity fluid cutoff time of $t = 20.0$ ms. During the initiation of vortex formation ($t = 15.0$–20.0 ms), the stretching term of fuel dilution contributes less to the increase of flow vorticity than in the other dilution conditions. As a single vortex moves downstream, the stretching effect develops differently than in the other conditions.

The overall effect of volumetric expansion on the change in total circulation is represented in Fig. 10(b). The volumetric expansion terms for all dilution conditions are typically negative during the initiation of vortex formation, which means that volumetric expansion affects the attenuation of the flow vorticity. In the fuel dilution, the destructive effect on the vorticity is greater than in the other dilution conditions until 20.0 ms. This is because the increase in entrainment of the surrounding and high-temperature fluids inside the single vortex significantly affects the volumetric

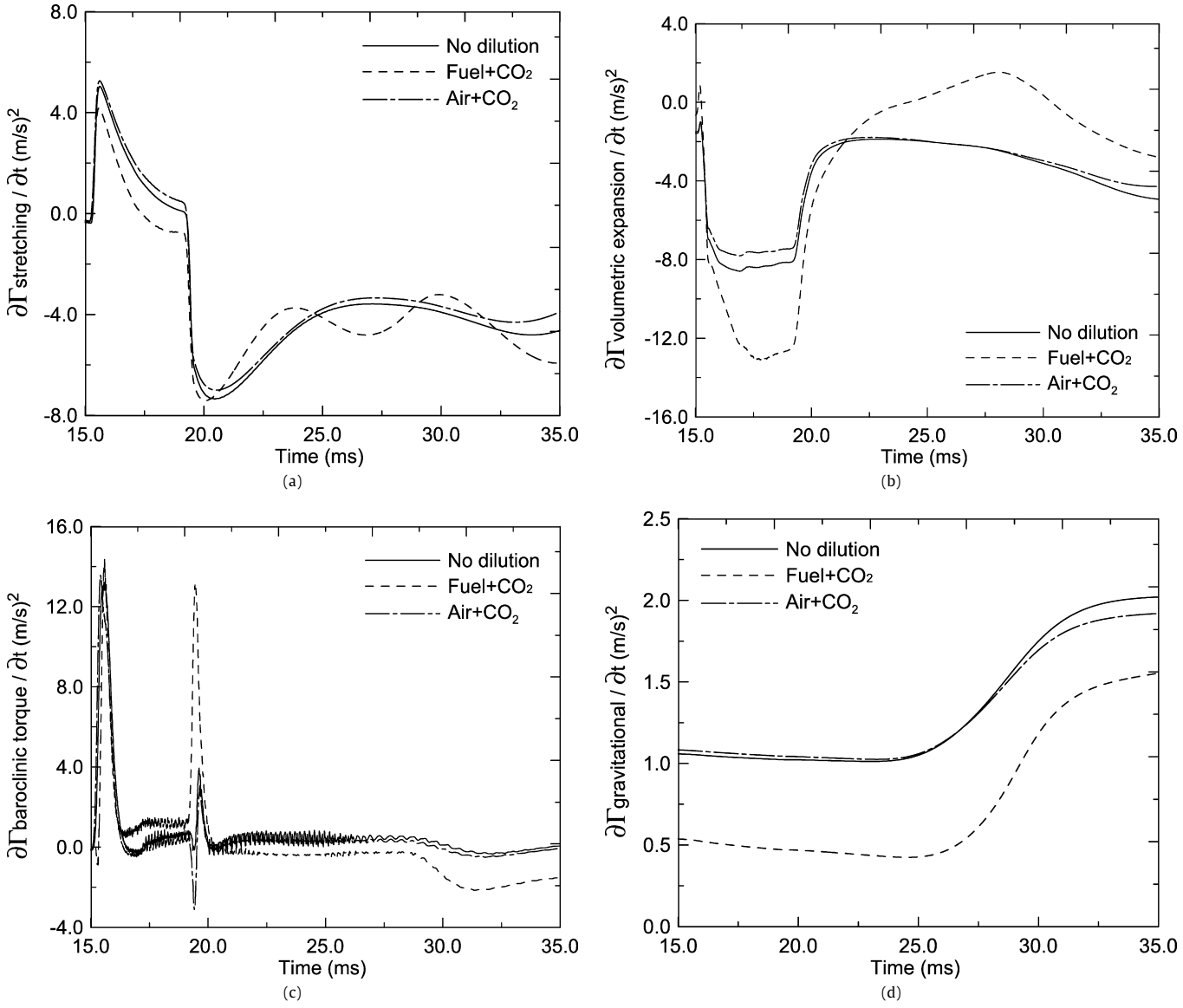

Fig. 10. Contributions to the change in total circulation over time for dilution conditions from the terms in Eq. (15) related to the following: (a) Stretching, (b) volumetric expansion, (c) baroclinic torque, and (d) gravitational term.

expansion. However, in fuel dilution, after 20.0 ms, uniform temperature distribution inside the single vortex due to increase in mixing rate reduces the effect of volumetric expansion on vortical flow field compared to other dilution conditions.

Fig. 10(c) indicates that the baroclinic torque term for all dilution conditions contributes primarily to the generation of vorticity during the initiation of vortex formation. In addition, this term plays the most important role for the change in total circulation compared to other terms, with the exception of the viscous terms. The significant increase in the baroclinic torque terms at 20.0 ms, for the fuel dilution, can be attributed mainly to the change in density gradient inside the vortex as a result of CO_2 dilution in the fuel stream. Nevertheless, the single vortex for all dilution conditions is likely to have a similar pressure distribution as estimated from the vortex shapes in Fig. 5. Consequently, the baroclinic torque term for fuel dilution is more important to the generation of vorticity than in the other dilution conditions. As a single vortex develops downstream, however, the baroclinic torque term for fuel dilution contributes mainly to the attenuation of vorticity, while the corresponding terms in the other dilution conditions exert little influence on the rate of change in total circulation.

The contribution of the gravitational term to the change in total circulation is shown in Fig. 10(d). The gravitational effect, which depends on the radial density gradient in all dilution conditions, is initially constant, and it gradually increases at 25.0 ms. The effect for fuel dilution is not larger than in other dilution conditions since CO_2 dilution causes a very small change in fuel density (1.11 kg/m^3 at inlet) and oxidizer density (1.17 kg/m^3). The density difference between fuel and oxidizer in no dilution is less than in air dilution, but the generation effect on vorticity in no dilution is greater than in air dilution because the flame temperature for no dilution is higher than in air dilution, as shown in Fig. 10(d). Although the effect of viscosity-related term on the change in total circulation was not presented in the paper, a comparison of the three dilution conditions did not reveal any significant difference on viscosity-related terms except that the effect in fuel dilution is slightly greater than in the other cases. In result, the change of dynamic viscosity due to CO_2 dilution has little effect on vorticity generation and attenuation.

Further studies related to the flame-vortex interaction under various conditions are essential to investigate the specific effect of CO_2 dilution in a turbulent flame. Furthermore, in the present study, we have observed only a single vortex generated at a fuel nozzle with specific impulsive intensity, but, if we can expand the simulation to include control of the location and impulsive intensity of vortex generation as well as the amount of CO_2 dilution, the methodology of the present study may prove useful for elucidating the hydrodynamic effects of CO_2 dilution on turbulent flames.

4. Conclusions

The effects of CO_2 dilution on a single vortex in a CH_4–air nonpremixed jet flame have been numerically investigated. We draw the following conclusions from analyses of vortex dynamics interacting with flame-diluted CO_2:

The CO_2 dilution in fuel stream results in an increased momentum flux leading to a larger vortex radius and greater entrainment of surrounding fluid than in the other dilution conditions. Thus, the dilution of CO_2 in the fuel stream enhances mixing inside the single vortex and increases the stretching of the flame surface. Therefore, the interaction between flame and vortex appears to be more important in fuel dilution than in no dilution and air dilution.

Regarding the contributions to the change in total circulation, the results show that, in the stage of vortex formation, the vorticity-generating effect of the baroclinic torque term and the vorticity-attenuating effect of the volumetric expansion term are greater in fuel dilution than in the other dilution conditions during vortex formation. However, after vortex formation, these terms show the opposite tendencies. In addition, the effects of CO_2 dilution on the stretching, gravitational, and viscous terms have little influence on total circulation except for causing minor variation among the dilution conditions.

The present study, which uses flame-vortex interaction to investigate the effects of CO_2 dilution, is expected to give good implications on the hydrodynamic effects by CO_2 dilution in turbulent flame, if the location and impulsive intensity of vortex generation, and the amount of CO_2 dilution, can be adequately controlled.

Acknowledgements

This work is sponsored by the Combustion Engineering Research Center (CERC) of Korea.

References

[1] E.B. Charles, Oxygen-Enhanced Combustion, CRC Press, 1998.
[2] C.E. Lee, C.H. Hwang, An experimental study on the flame stability of LFG and LFG-mixed fuels, Fuel 86 (2007) 649–655.
[3] J.R. Bae, B.J. Lee, Effect of diluents and oxygen-enrichness on the stability of nonpremixed flame, in: Proc. KSME 2002 Spring Annual Meeting B, 2002, pp. 2019–2024.
[4] N. Saito, Y. Ogawa, Y. Saso, C. Liao, R. Sakei, Flame-extinguishing concentrations and peak concentrations of N_2, Ar, CO_2 and their mixtures for hydrocarbon fuels, Fire Safety J. 27 (1996) 185–200.
[5] C.E. Lee, S.R. Lee, J.W. Han, J. Park, Numerical study on effect of CO_2 in flame structure and NOx formation of CH_4–air counterflow diffusion flame, Int. J. Energy Research 24 (2000) 2–12.
[6] J.W. Han, C.E. Lee, Numerical study on flame structure and NO formation characteristics in oxidizer-controlled diffusion flames, Trans. KSME B 26 (5) (2002) 742–749.
[7] H. Liu, H. Guo, G.J. Smallwood, O.L. Gulder, The chemical effects of carbon dioxide as an additive in an ethylene diffusion flame: implications for soot and NOx formation, Combust. Flame 125 (2001) 778–787.
[8] S.J. Chen, W.J.A. Dahm, J.A. Silver, G. Tryggvason, Concentration fields of reactant and products species in a reacting vortex ring, in: 39th Aero. Sci. Meeting & Exhibit, AIAA, 2001, pp. 1–5.
[9] W.J.A. Dahm, S.J. Chen, J.A. Silver, Turbulent flame processes via diffusion flame-vortex ring interactions, in: 6th Int. Microgravity Combust. Workshop, 2001, pp. 65–68.
[10] F. Takahashi V.R. Katta, Numerical experiments on the vortex-flame interactions in a jet diffusion flame, in: 31st Aero. Sci. Meeting & Exhibit, AIAA 93-0456, 2003.
[11] S. James, C.K. Madnia, Direct numerical simulation of a laminar vortex ring, Phys. Fluids 8 (9) (1996) 2400–2414.
[12] J.S. Hewett, C.K. Madnia, Flame-vortex interaction in a reacting vortex ring, Phys. Fluids 10 (1) (1998) 189–205.
[13] P.A. McMurtry, W.H. Jou, J.J. Riley, R.W. Metcalfe, Direct numerical simulations of a reacting mixing layer with chemical heat release, AIAA J. 24 (6) (1985) 962–970.
[14] R.J. Kee, G. Dixon-Lewis, J. Warnatz, E. Coltrin, J.A. Miller, A Fortran computer code package for the evaluation of gas-phase multicomponent transport properties, Sandia Report, SAND86-8246, 1986.
[15] B.P. Leonard, A stable and accurate convective modeling procedure based on quadratic upstream interpolation, Comput. Methods Appl. Mech. Engrg. 19 (1979) 59–98.
[16] H.N. Najm, P.S. Wyckoff, Premixed flame response to unsteady strain rate and curvature, Combust. Flame 110 (1997) 92–112.
[17] C.W. Hirt, J.L. Cook, Calculating three-dimensional flows around structures and over rough terrain, J. Comp. Phys. 10 (1972) 324–340.
[18] R.J. Kee, F.M. Rupley, J.A. Miller, Chemkin-II: a Fortran chemical kinetic package for the analysis of gas phase chemical kinetics, Sandia Report, SAND89-8009B, 1989.
[19] C.B. Oh, C.E. Lee, J. Park, Numerical investigation of extinction in a counterflow nonpremixed flame perturbed by a vortex, Combust. Flame 138 (2004) 225–241.
[20] C.B. Oh, Direct numerical simulation on the interaction of counterflow nonpremixed flame and a single vortex, Ph.D. Dissertation, Inha University, 2003.
[21] V. Dupont, M. Pourkashanian, A. Williams, Modeling of process heaters fired by natural gas, Inst. Energy 66 (1993) 20–28.
[22] N. Peters, Laminar diffusion flamelet models in non-premixed turbulent combustion, Prog. Energy Combust. Sci. 10 (1984) 310–339.
[23] A. Hamins, B. Matthew, C.B. Oh, S.C. Kim, Effect of buoyancy on the radiative extinction limit of low-strain-rate nonpremixed methane–air flame, Combust. Flame 151 (2007) 225–234.
[24] C.B. Oh, A. Hamins, M. Bundy, J. Park, The two-dimensional structure of low strain rate counterflow nonpremixed flames in normal and microgravity, Combust. Theory Modeling 12 (2) (2008) 283–302.